Electronic Supplementary Material (ESI) for Inorganic Chemistry Frontiers.

Supporting Information

Magnetoelectric Synergy Strategy for Superior Iron Disulfide Anode

Yaoyao Xiao[a,b], Yihui Liu[a,b], Bingbing Liu[a,b], Zhenguo Qi[a,b], Youbin Zhang[a,b], Fusheng Liu[a,b]* and Guohui Qin[a,b]*

[a] *State Key Laboratory Base for Eco-Chemical Engineering, College of Chemical Engineering, Qingdao University of Science and Technology, Qingdao 266042, Shandong, China*

[b] *Shandong Synergetic Innovation Center of Ecological and Chemical Engineering, Qingdao 266042, China*

Corresponding author.

E-mail address:guohuiq163@sina.com

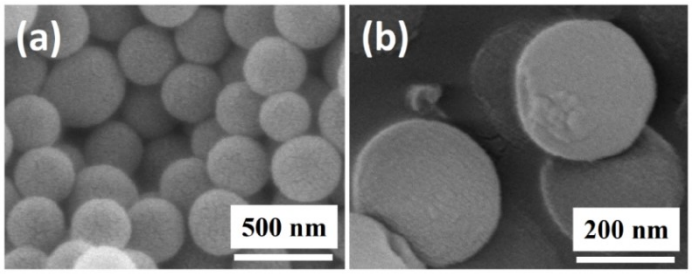

Fig. S1. SEM images of Fe_3O_4/C sample.

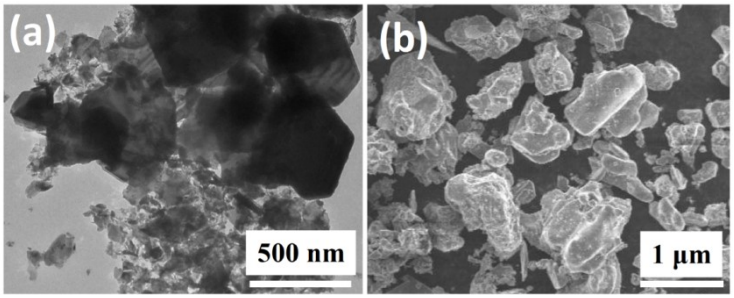

Fig. S2. (a) TEM and (b) SEM images of FeS_2 sample.

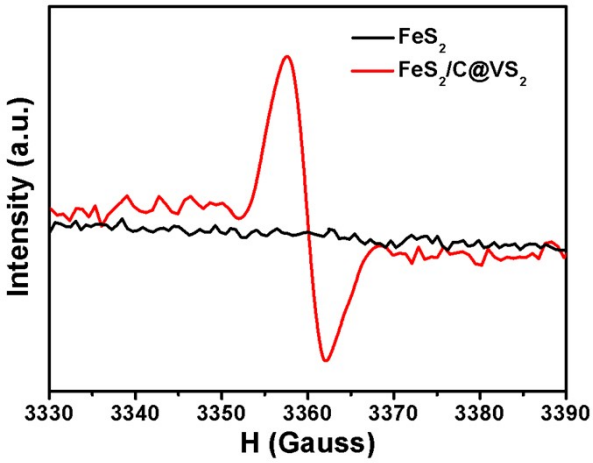

Fig. S3. EPR image of FeS_2 and FeS_2/C@VS_2 samples.

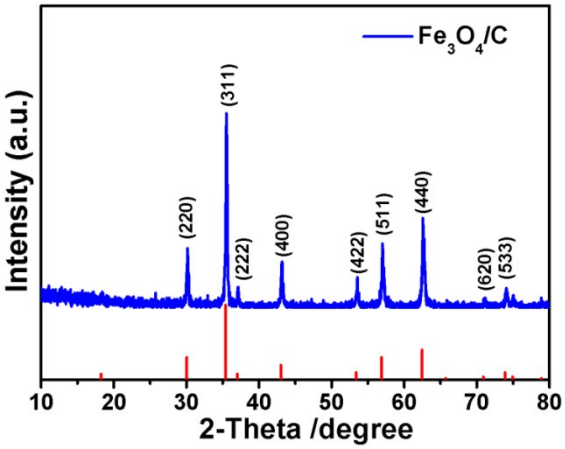

Fig. S4. XRD pattern spectra of Fe_3O_4/C sample.

The sharp crystalline peaks at 2θ of 30.1°, 35.5°, 37.0°, 43.3°, 53.3°, 57.3°and 62.9°can be well attributed to (220), (311), (222), (400), (422), (511) and (440) planes of Fe_3O_4 (PDF# 19-0629).[1]

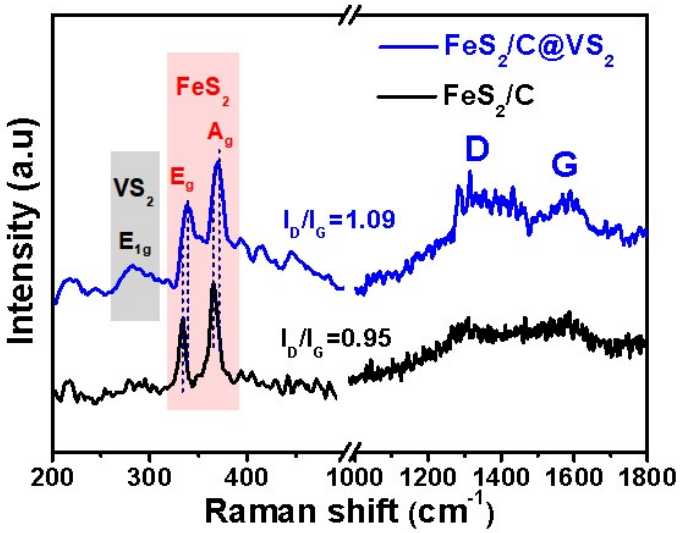

Fig. S5. Raman spectra of FeS_2/C@VS_2 and FeS_2/C samples.

In the raman spectra of FeS_2/C@VS_2, two peaks located at 1314 and 1589 cm^{-1} can be observed corresponding to the D and G peaks of the carbon. The characteristic peaks located at 337.79 and 370.13 cm^{-1} corresponded to the E_g vibration mode of S atoms and the A_g vibration mode of S-S phase stretching in FeS_2. The characteristic peak located at 283.61 cm^{-1} corresponded to E_{1g} vibration mode of VS_2. Compared with FeS_2/C, the higher I_D:I_G value of FeS_2/C@VS_2 implied its affluent defective active sites after the coupling of VS_2.

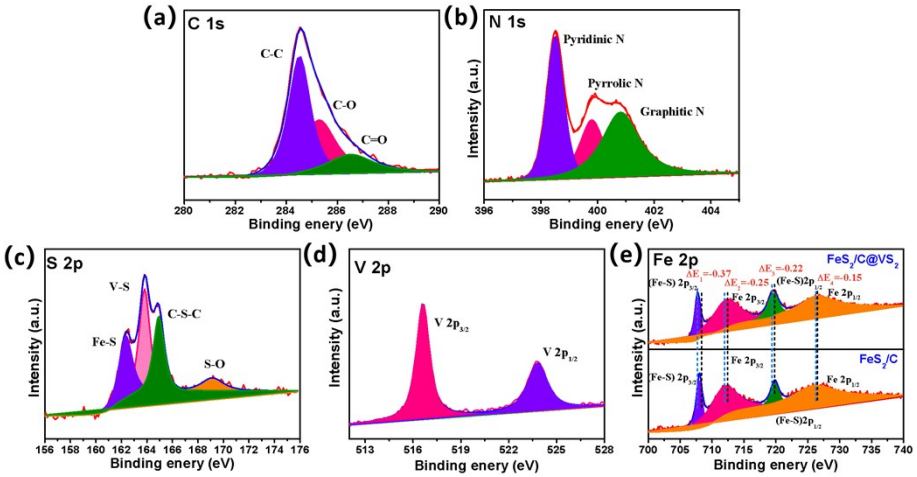

Fig. S6. XPS survey spectrum of FeS_2/C@VS_2 sample, the high-resolution spectrum of (a) C 1s, (b) N 1s, (c) S 2p and (d) V 2p. Comparison of (e) Fe 2p spectrum with FeS_2/C and FeS_2/C@VS_2 samples.

The C 1s spectra exhibited three peaks located at 284.53, 285.33 and 286.55 eV corresponding to the binding energies of C-C, C-O and C=O, respectively. The peaks of pyridinic N, pyrrolic N and graphitic N were plotted at 398.51 eV, 399.79 eV and 400.75 eV, respectively. The peaks located at 162.35 eV and 163.82 eV was originated from the FeS_2@VS_2 heterojunction, while the C-S-C peak located at 164.92 eV further demonstrated the tight bonding of the carbon with the sulfide. The last peak located at 169.21 eV was assigned to S-O. The V peaks at 516.6 and 523.7 eV are ascribed to V $2p_{3/2}$ and V $2p_{1/2}$, corresponding to the V^{4+} oxidation state.

The peak of (Fe-S) $2p_{3/2}$, Fe $2p_{3/2}$, (Fe-S) $2p_{1/2}$ and Fe $2p_{1/2}$ in the FeS_2/C shifted from the high-energy region (708.06, 712.44, 719.80 and 726.49 eV) to the low-energy region (707.69, 712.19, 719.58 and 726.34 eV) in FeS_2/C@VS_2 (ΔE_1=-0.37 eV, ΔE_2=-0.25 eV, ΔE_3=-0.22 eV, ΔE_4=-0.15 eV). The shift of the binding energy in the intimate heterojunction material confirmed that the electrons can be transferred from VS_2 to FeS_2 arisen from the build-in electronic-field between FeS_2/C and VS_2.[3]

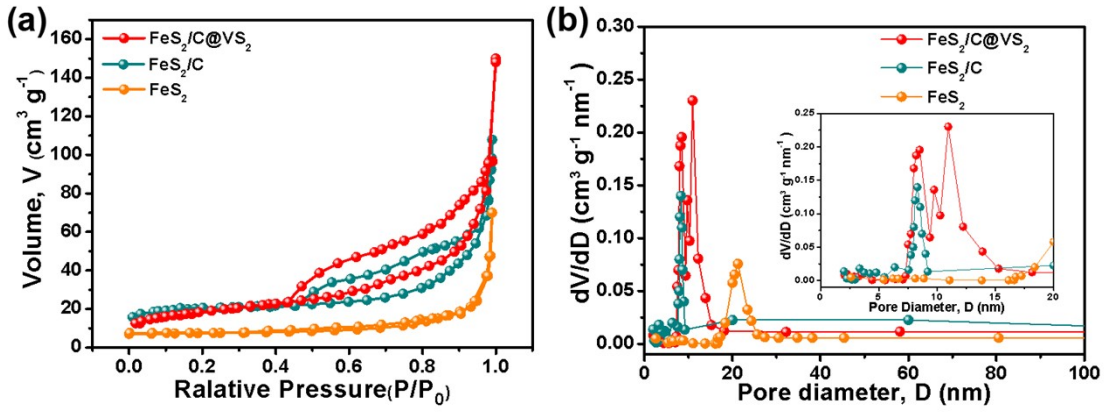

Fig. S7. (a) Nitrogen adsorption-desorption isotherms and (b) pore size distribution profiles of the FeS_2, FeS_2/C and FeS_2/C@VS_2 samples.

The specific surface area and pore size distribution of the sample can be further investigated accurately by N_2 adsorption-desorption analysis. From the isothermal curves, it can be obtained that the FeS_2/C@VS_2 had larger absorbance than that of FeS_2 and FeS_2/C, indicating that the FeS_2 multi-particle and VS_2 nanoflowers provided a high specific surface area of 102.8 m^2 g^{-1}, and there were hysteresis loops in both curves, which were consistent with the type isothermal IV-curve. Therefore, it was a typical mesoporous structure. The hysteresis loops were closely related to the form of pores, and the hysteresis loop of FeS_2/C@VS_2 was HI type, indicating that its was cumulate pores composed of nanoparticles, which was consistent with the results of TEM images. Also, its pore size was about 7-15 nm, this structure can promote the electrolyte ion transport during the electrochemical process and thus improved the rate performance of the battery.

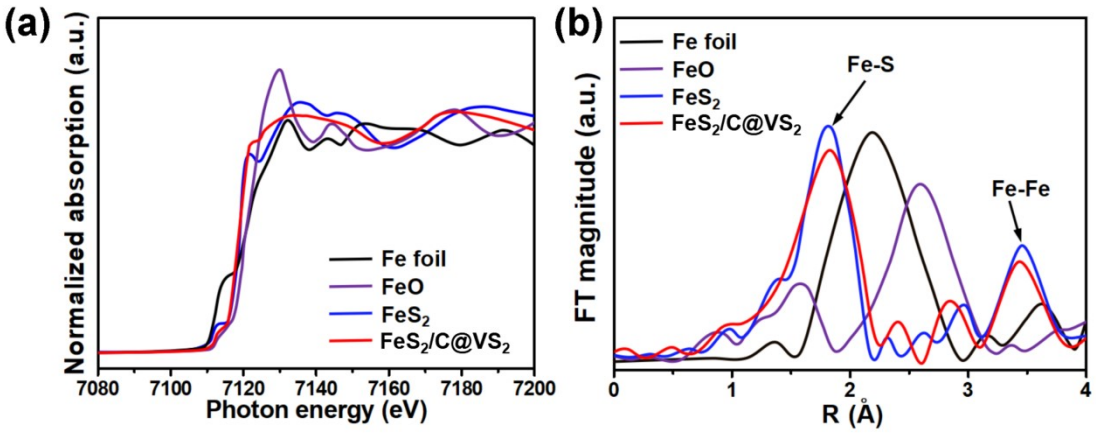

Fig. S8. (a) Comparison of Fe K-edge XANES spectra and (b) Fourier transform of the EXAFS spectra of Fe foil, FeO, FeS_2 and FeS_2/C@VS_2 samples.

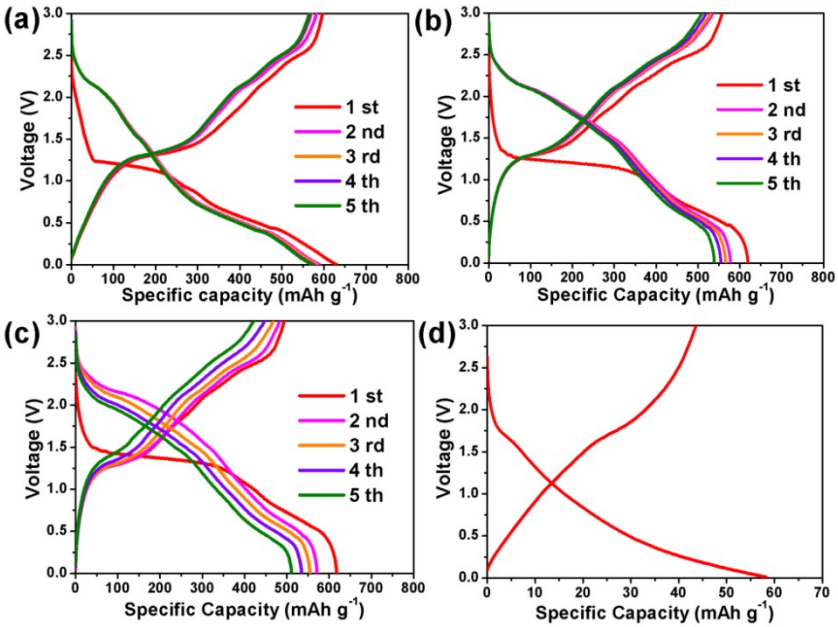

Fig. S9. Galvanostatic discharge/charge curves of (a) FeS_2/C@VS_2, (b) FeS_2/C, (c) FeS_2 and (d) VS_2 in the initial loops.

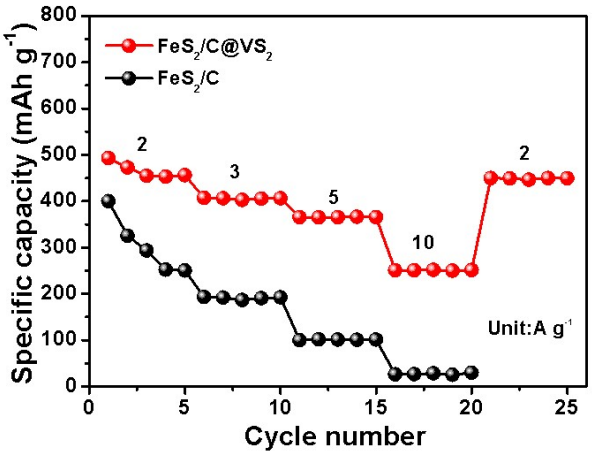

Fig. S10. Rate capability of FeS_2/C and FeS_2/C@VS_2 electrodes at high current densities.

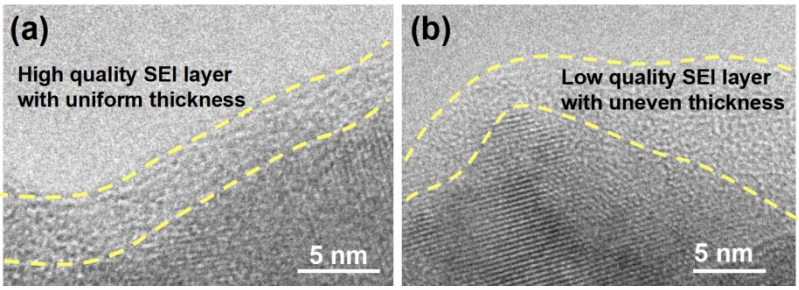

Fig. S11. TEM images of (a) $FeS_2/C@VS_2$ and (b) FeS_2/C electrodes after cycles.

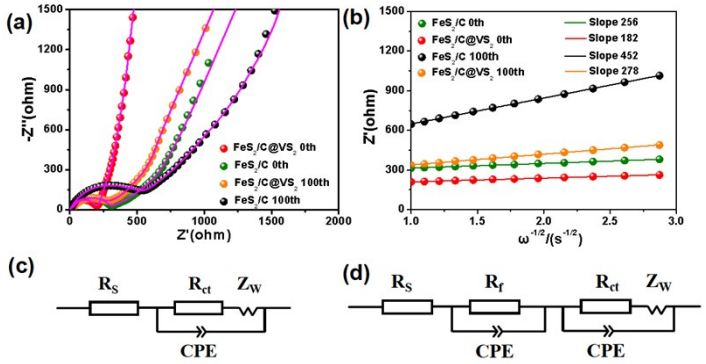

Fig. S12. (a) EIS plots of FeS_2/C and FeS_2/C@VS_2 electrodes before and after 100 cycles, (b) corresponding linear fits of the Z′ versus $\omega^{-1/2}$ in the low-frequency region. The corresponding equivalent circuit model (c) before and (d) after 100 cycles.

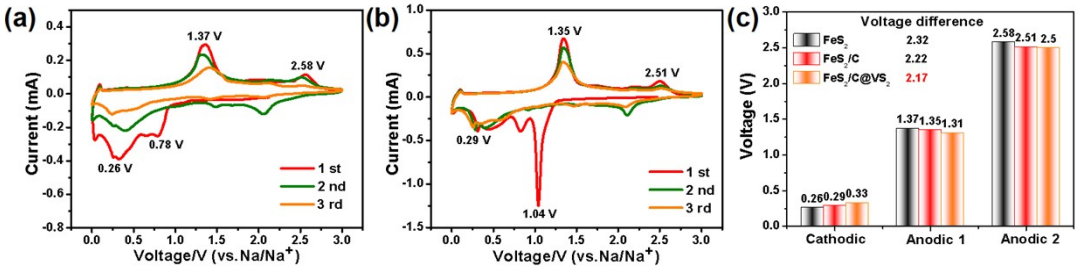

Fig. S13. Cyclic voltammograms of (a) FeS_2 and (b) FeS_2/C electrodes, (c) comparison of peak voltages of FeS_2-based electrodes.

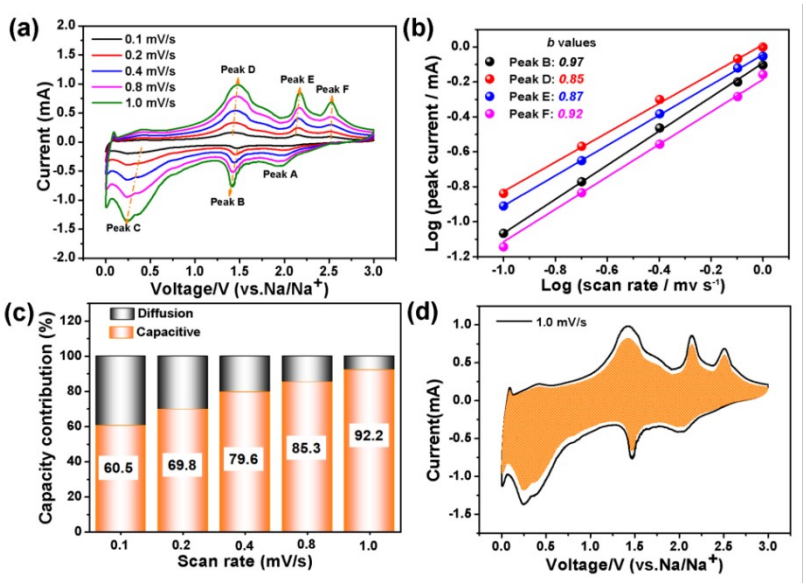

Fig. S14. (a) CV curves at various scan rates from 0.1 to 1.0 mV s^{-1}, (b) the plots of log(i) vs. log(v), (c) the ratios of capacitive contribution at various rates, (d) CV curves with capacitive contribution at 1.0 mV s^{-1} of FeS_2/C@VS_2.

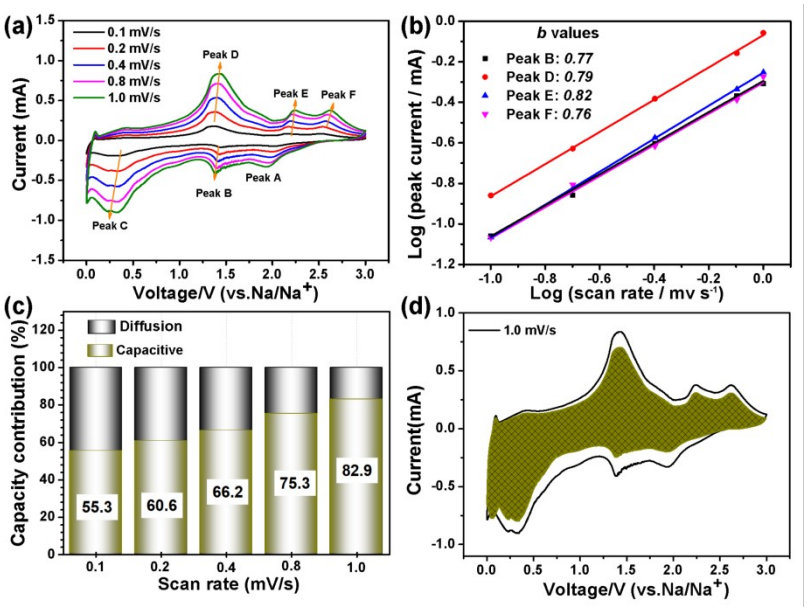

Fig. S15. (a) CV curves at various scan rates from 0.1 to 1.0 mV s^{-1}, (b) the plots of log(i) vs. log(v), (c) the ratios of capacitive contribution at various rates, (d) CV curves with capacitive contribution at 1.0 mV s^{-1} of FeS_2/C.

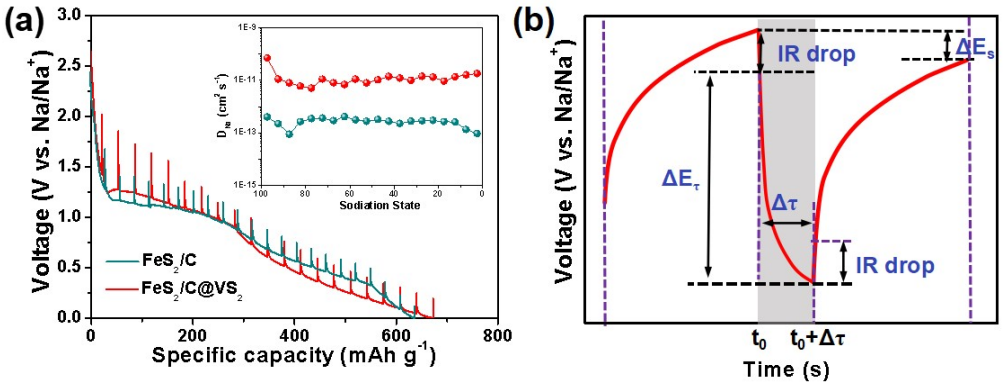

Fig. S16. (a) Discharge curves of the GITT test for FeS_2/C and FeS_2/C@VS_2 electrodes and comparison of the corresponding Na^+ diffusion coefficient. (b) The detailed voltage response during a single current pulse.

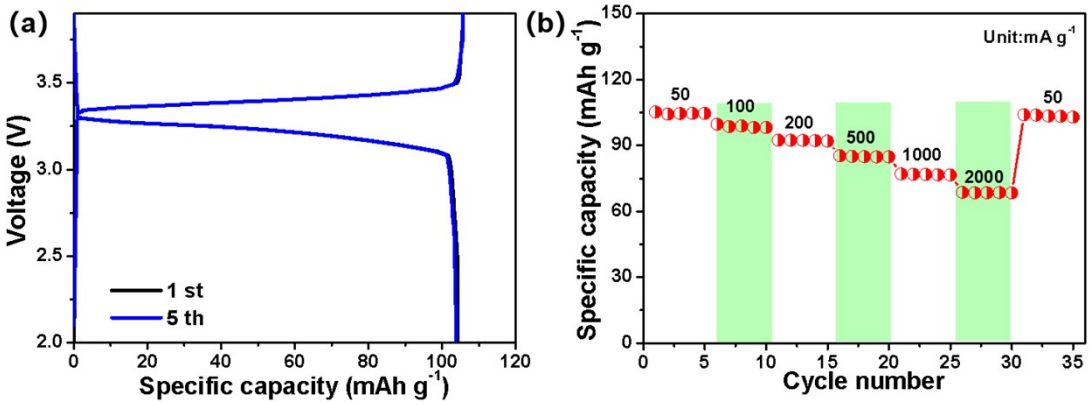

Fig. S17. The electrochemical performance of NVP/C cathodes. (a) Galvanostatic charge-discharge curves, (b)rate capacity.

The NVP/C cathodes were tested with a voltage window of 2.0-3.9 V under 0.05 A g^{-1}, it displayed a discharge capacity of 104.3 mA h g^{-1} in the first loop. With the elevating current density from 0.05 to 2.0 A g^{-1}, it showed excellent rate behaviors with average discharge capacities of 104.7, 98.7, 92.3, 85.0, 75.8 and 68.5 mA h g^{-1}, respectively.

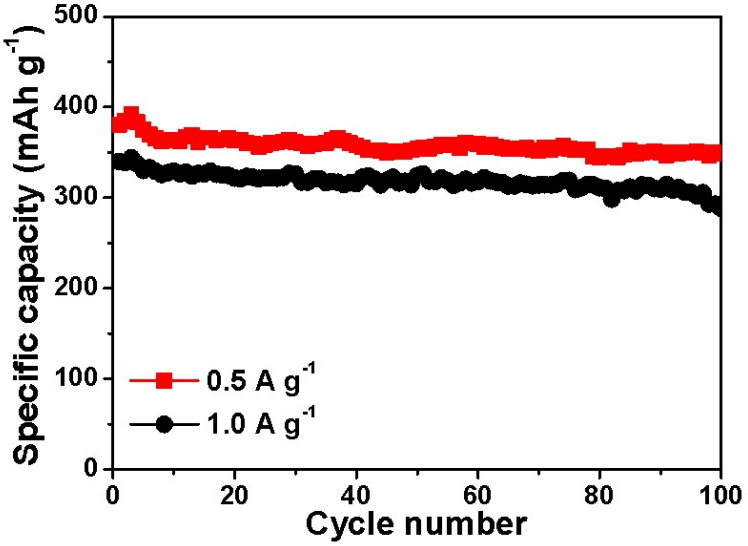

Fig. S18. The cycling performance at 0.5 and 1.0 A g^{-1} of the full cells.

Table S1. Composition content (wt%) of FeS_2/C@VS_2 sample obtained by ICP-MS.

	FeS_2	VS_2	C
Content(%)	73.2	15.2	11.6

Table S2. The kinetic parameters of FeS_2/C and FeS_2/C@VS_2 samples after 100 cycles.

Materials	Cycle	R_s	R_f	R_{ct}
FeS_2/C	0	5.53	-	300.95
	100	7.62	11.63	589.67
FeS_2/C@VS_2	0	4.71	-	198.69
	100	5.76	8.69	320.26

Table S3. A comprehensive comparison with the recent references involving various Fe-based electrodes for SIBs.

Materials	**Current rate (A g^{-1})**	**Capacity (mAh g^{-1})**	**High current rate (A g^{-1})**	**Capacity (mAh g^{-1})**	**Ref.**
FeS_2/MoS_2-rGO	0.1	460	2	380	4
Core-shell FeS@carbon	0.1	498	2	295	5
FeS_2@C nanoboxes	0.1	560	2	470	6
FeS_2/C nanospheres	0.1	400	-	-	7
FeS@C-N microspheres	0.1	656	0.8	365	8
FeS_2@C nanorods	0.1	365	2	235	9
FeS_2@$FeSe_2$ microspheres	0.1	596	2	426	10
$FeS_{2-x}Se_x$	0.1	370	2	264	11
FeS_2@G@CNF	0.1	436	2	312	12
FeS_2/C@VS_2	**0.1**	**542**	**2**	**453**	**This work**

References:

1. W. Ma, P. He, T. Wang, J. Xu, X. Liu, Q. Zhuang, Z.-K. Cui and S. Lin, Microwave absorption of carbonization temperature-dependent uniform yolk-shell H-Fe_3O_4@C microspheres, *Chem. Eng. J.*, 2021, **420**, 129875.

2. Z. Feng, G. Li, X. Wang, C. J. Gómez-García, J. Xin, H. Ma, H. Pang and K. Gao, FeS_2/MoS_2@RGO hybrid materials derived from polyoxomolybdate-based metal-organic frameworks as high-performance electrocatalyst for ammonia synthesis under ambient conditions, *Chem. Eng. J.*, 2022, **445**, 136797.

3. L. Cao, X. Gao, B. Zhang, X. Ou, J. Zhang and W.-B. Luo, Bimetallic Sulfide Sb_2S_3@FeS_2 Hollow Nanorods as High-Performance Anode Materials for Sodium-Ion Batteries, *ACS Nano*, 2020, **14**, 3610-3620.

4. S. Yuvaraj, G. K. Veerasubramani, M.-S. Park, P. Thangavel and D.-W. Kim, Facile synthesis of FeS_2/MoS_2 composite intertwined on rGO nanosheets as a high-performance anode material for sodium-ion battery, *J. Alloys Compd.*, 2020, **821**, 153222.

5. F. Bu, P. Xiao, J. Chen, M. F. Aly Aboud, I. Shakir and Y. Xu, Rational design of three-dimensional graphene encapsulated core-shell FeS@carbon nanocomposite as a flexible high-performance anode for sodium-ion batteries, *J. Mater. Chem. A.*, 2018, **6**, 6414-6421.

6. Z. Liu, T. Lu, T. Song, X.-Y. Yu, X. W. Lou and U. Paik, Structure-designed synthesis of FeS_2@C yolk-shell nanoboxes as a high-performance anode for sodium-ion batteries, *Energy Environ. Sci.*, 2017, **10**, 1576-1580.

7. Y. Zhu, L. Suo, T. Gao, X. Fan, F. Han and C. Wang, Ether-based electrolyte enabled Na/FeS_2 rechargeable batteries, *Electrochem. Commun.*, 2015, **54**, 18-22.

8. Z.-G. Wu, J.-T. Li, Y.-J. Zhong, J. Liu, K. Wang, X.-D. Guo, L. Huang, B.-H. Zhong and S.-G. Sun, Synthesis of FeS@C-N hierarchical porous microspheres for the applications in lithium/sodium ion batteries, *J. Alloys Compd.*, 2016, **688**, 790-797.

9. Z. Lu, N. Wang, Y. Zhang, P. Xue, M. Guo, B. Tang, Z. Bai and S. Dou, Pyrite FeS_2@C nanorods as smart cathode for sodium ion battery with ultra-long lifespan and notable rate performance from tunable pseudocapacitance, *Electrochim. Acta.*, 2018, **260**, 755-761.

10. W. Zhao, C. Guo and C. M. Li, Lychee-like FeS_2@$FeSe_2$ core-shell microspheres anode in sodium ion batteries for large capacity and ultralong cycle life, *J. Mater. Chem. A.*, 2017, **5**, 19195-19202.

11. Y. Long, J. Yang, X. Gao, X. Xu, W. Fan, J. Yang, S. Hou and Y. Qian, Solid-Solution Anion-Enhanced Electrochemical Performances of Metal Sulfides/Selenides for Sodium-Ion Capacitors: The Case of $FeS_{2-x}Se_x$, *ACS Appl. Mater. Inter.*, 2018, **10**, 10945-10954.

12. C. Chen, Y. Yang, X. Tang, R. Qiu, S. Wang, G. Cao and M. Zhang, Graphene-Encapsulated FeS_2 in Carbon Fibers as High Reversible Anodes for Na^+/K^+ Batteries in a Wide Temperature Range, *Small*, 2019, **15**, 1804740.